

Ultra Lightweight Image Super-Resolution with Multi-Attention Layers

Abdul Muqeet¹, Jiwon Hwang¹, Subin Yang¹, JungHeum Kang¹, Yongwoo Kim^{2*}, and Sung-Ho Bae^{1*}

¹ Dept. of Computer Science and Engineering, Kyung Hee University, South Korea
 {amuqeet,jiwon.hwang,ysb8049, chhkang123,shbae}@khu.ac.kr

² Dept. of System Semiconductor Engineering, Sangmyung University, South Korea
 yongwoo.kim@smu.ac.kr

Abstract. Lightweight image super-resolution (SR) networks have utmost significance for real-world applications. There are several deep learning based SR methods with remarkable performance, but their memory and computational cost are hindrances in practical usage. To tackle this problem, we propose a Multi-Attentive Feature Fusion Super-Resolution Network (MAFFSRN). MAFFSRN consists of proposed feature fusion groups (FFGs) that serve as a feature extraction block. Each FFG contains a stack of proposed multi-attention blocks (MAB) that are combined in a novel feature fusion structure. Further, the MAB with a cost-efficient attention mechanism (CEA) helps us to refine and extract the features using multiple attention mechanisms. The comprehensive experiments show the superiority of our model over the existing state-of-the-art. We participated in AIM 2020 efficient SR challenge with our MAFFSRN model and won 1st, 3rd, and 4th places in memory usage, floating-point operations (FLOPs) and number of parameters, respectively.

Keywords: Super-Resolution, Feature Extraction, Multi-Attention, Low-computing Resources, Lightweight Convolutional Neural Networks

1 Introduction

This paper focuses on the single image super-resolution (SISR) problem. In SISR we aim to reconstruct a high-resolution (HR) image from a low-resolution (LR) image. We refer super-resolution (SR) as interchangeably with SISR in remaining of the paper. According to [47], SISR problem can be mathematically written as,

$$I_{LR} = (I_{HR} \otimes k) \downarrow_s + n, \quad (1)$$

* co-corresponding authors

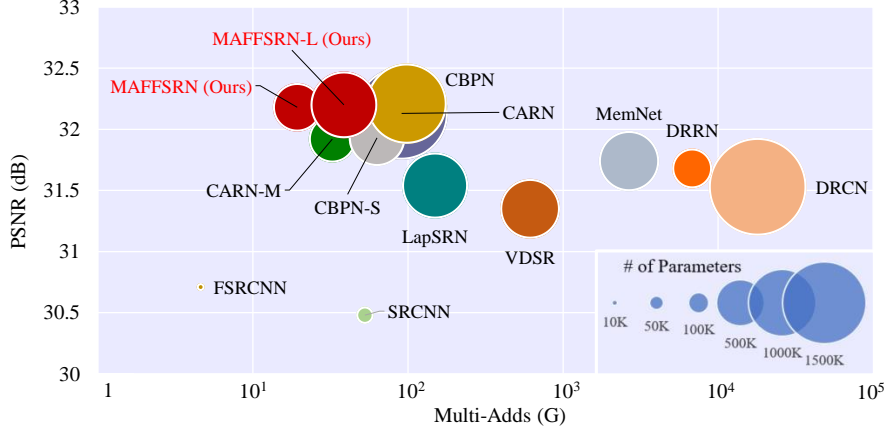


Fig. 1: Performance comparison of existing lightweight methods on Set5 [3] (4 \times). Multi-adds are calculated on 720p HR image. The results show the superiority of our models among existing methods

where I_{LR} and I_{HR} refer to given input LR and desire HR images. ‘ k ’ in Eq. 1) denotes as a blur kernel, \downarrow_s represents a down-scaling operator, and ‘ n ’ is a Gaussian noise. By following previous works, we assume that images are down-sampled with bicubic interpolation [2][52].

There are multiple mapping solutions possible from single LR to HR images that make this problem ill-posed. Albeit of its ill-posedness, the deep learning methods like [8,10,22] have shown notable success in this domain. For instance, SRCNN [8] with only three layers outperformed the previous non-deep learning methods. Subsequently, deeper and complex architectures have been proposed to improve the performance of SR methods [2,29,13,50,51]. In spite of their outstanding performance, such methods are impracticable for real-world applications because of their large memory size, number of operations, and parameters.

Numerous lightweight models have been proposed to resolve these issues. CARN [2] introduces a lightweight and efficient cascaded residual network with several residual connections. FALSR [7] employs a network architecture search (NAS) technique rather than manually searching it in SISR domain. CBPN [52] proposed an efficient version of the DBPN network [13] that emphasizes the importance of high-resolution features of LR images. These models were designed to reduce the computational cost, though all of these come with their smaller version of models, such as, CARN-M[2], CBPN-S[52], FALSR-B, and FALSR-C[7]. Hence, it shows that their original models are inadequate for real-world application.

The need of such practical models motivated us to propose a lightweight model called MAFFSRN. Its computation cost is similar to CARN-M, CBPN-S, FALSR-B, FALSR-C [2,52,7], but matches the performance of their corresponding original models. With the comprehensive experiments, we show that our

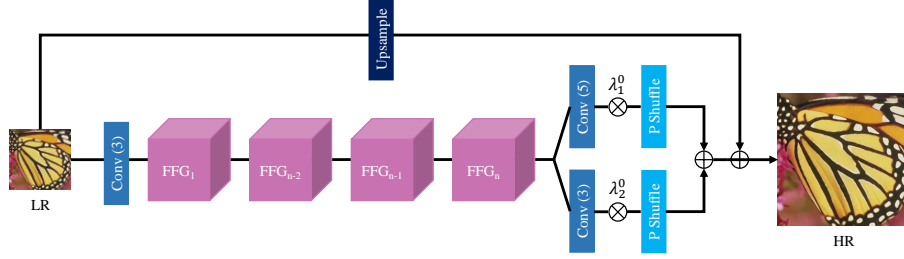


Fig. 2: Our main network architecture (MAFFSRN). It consists of stack of FFG where each FFG has multiple MAB combined with modified BFF. Conv (3) and Conv (5) refer to 3×3 and 5×5 convolutions, respectively, P Shuffle means pixel shuffle [34]. Each lambda (λ) is trainable scalar parameter. Lastly, we add up-sampled LR image to the reconstructed output

models achieve the best performance on all of the benchmark datasets. Further, we introduce a large model (MAFFSRN-L) to compare performance with heavy state-of-the-art methods. Note that its size still remains smaller than existing efficient models. We show our benchmark results in Figure 1.

Our model is specifically aimed to minimize the computation cost such as floating point operations (FLOPs) and memory consumption but maximize the network performance. To increase the network performance, we utilize the feature fusion group (FFG) that consists of several multi-attention blocks (MAB). In SR deep network architectures the vital information is vanished during the flow of network [50]. Our method tackles this problem with FFG and MAB and results suggest that they enable us to increase the depth of network with minimal computational cost, consequently increasing the network performance. The next challenge is to minimize the computational cost and memory usage. For this purpose, we propose changes for the enhanced spatial attention (ESA) block [30]. First, we introduce cost-efficient (CEA) block to directly apply attention mechanism on the input features. Second, we replaced the Conv groups of ESA [30] with dilated convolutions to get benefit from the large spatial size. For the feature fusion structure, we found during the experiments that the performance of hierarchical feature fusion (HFF) [27] remains lower than the binarized feature fusion (BFF) [32]. We discuss the details of these experiments in ablations studies. We evaluate our method on benchmark datasets and compare the performance against existing methods.

Our overall contributions are summarized as follows: 1) we introduce a lightweight model consisting of modified BFF, MAB, and CEA modules, that outperforms existing methods. We participated in AIM 2020 SR challenge [46] where our model was ranked 1st in memory consumption, 3rd in FLOPS, and 4th in number of parameters. 2) We provide comprehensive qualitative and quantitative comparison results on the benchmark datasets with multiple scaling factors ($\times 2$, $\times 3$, and $\times 4$).

2 Related work

The remarkable success of deep neural networks in other computer vision tasks [17],[14],[6] encouraged SR community to apply deep learning techniques in SR domain. SRCNN [8] apply a shallow neural network and surpasses the performance of traditional and conventional non-deep learning based methods. As [39] shows that deep networks have shown better results than shallow networks, several methods followed this trend and proposed deeper networks. VDSR [21] proposed a 20 layers network consisting of global skip-connection that element-wise add the up-sampled LR image to the output reconstructed image. EDSR [29] improved the SRResNet [26], that was based on ResNet architecture[14], by removing the trivial layers or those layers which degrade the performance, such as Batch Normalization[20]. RDN introduced dense connections similar to DenseNet [18] and improved the performance with fewer parameters than EDSR[29]. Certainly, they have improved the image fidelity, such as PSNR or SSIM significantly, however, the constrained real-world environments having low-power computing devices require to focus on other metrics, such as number of parameters, memory consumption, FLOPs, latency time, etc.

Therefore, there is growing interest to build lightweight models that need to be accurate as well. One strategy is to adopt model compression techniques to compress the models [12,16]. In this paper, our focus is to develop a new network architecture to remedy this problem. Hence, we only discuss the previous works that address such issues in SR domain.

The progress of such lightweight architectures started from FSRCNN [10]. It improves the performance of SRCNN [8] by directly applying SR network to LR images rather than up-sampled input. It also decreases the inference time by removing the high-cost up-sampling layers. DRRN [35] utilized recursive layers to reduce the number of parameters while keeping the depth of the network. CARN [2] applied several residual connections and recursive layers to reduce computational cost. FALSr [7] introduced automated neural architecture search (NAS) strategies in SR domain to propose an SR model for constrained environment. CBPN [52] proposed an efficient version of DBPN network [13] by replacing the expensive up- and down- projection modules with pixel shuffle layers. We observed that all these methods focused on trade-off between performance and computation cost that led them to propose another smaller version of their model such as CBPN-S [52], CARN-M [2], FALSr-B [7]. However, our proposed method achieves better or comparable performance as their original models whereas the computational cost remains the same or lower compared to their lightweight versions.

3 Proposed Method

In this section, we describe the details of our proposed architecture. As shown in Figure 2, our network architecture consists of n FFGs that are stacked in a sequential way. The details of FFG are given section 3.1. We use one convolutional (Conv) layer before FFGs to extract the shallow features from input LR

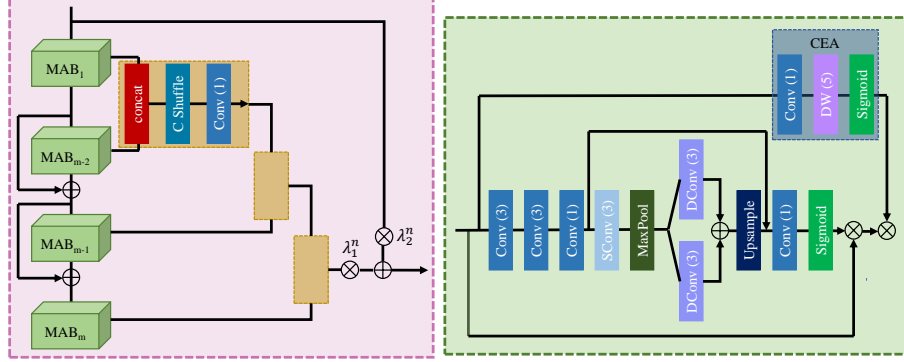


Fig. 3: Left figure shows structure of FFG and right figure shows MAB. ‘C Shuffle’ refers to channel shuffle, ‘SConv’ means strided convolution, ‘DConv’ means dilated convolution and ‘DW’ means depth-wise convolution. Parenthesis such as (1), (3) and (5) represents 1×1 , 3×3 , and 5×5 filters, respectively

image. Lastly, we apply couple of Conv layers with different filter sizes to extract multi-scale features that are followed by pixel-shuffle layers [34]. Further, motivated from [40], we add weights (denoted by λ_1^0 and λ_2^0) to both Conv layers to give weightage to the features and carry the weighted features to later layers. Later, the resultant information is element-wise added. Similar to [21], we element-wise add up-sample LR input into the output layer. Note, our overall architecture is primarily based on RDN architecture [51] that consists of local and global blocks.

For the given I_{LR} image, the shallow feature extraction step is given as

$$x_{sfe} = f_{sfe}(I_{LR}), \quad (2)$$

where f_{sfe} and x_{sfe} represent the 3×3 convolution and the resultant output, respectively. Next, for non-linear mapping or deep feature extraction step, we apply the stack of FFG as follows

$$x_{dfe} = f_{FFG}^n(f_{FFG}^{n-1}(\dots f_{FFG}^0(x_{sfe}))), \quad (3)$$

where f_{FFG}^n and x_{dfe} denote the n_{th} FFG and output of deep feature extraction step, respectively. Lastly, the reconstruction stage is given as

$$I_{SR} = f_{ps}(\lambda_1^0 f_5(x_{dfe})) + f_{ps}(\lambda_2^0 f_3(x_{dfe})) + f_{up}(I_{LR}), \quad (4)$$

where the details of notations in Eq. 4 are as follows: I_{SR} represents the desired SR image, f_3 and f_5 denote 3×3 and 5×5 convolutions, respectively, f_{ps} shows pixel-shuffle layer [34], f_{up} represent an up-sampling layer and λ_1^0 and λ_2^0 denote trainable scalar parameters.

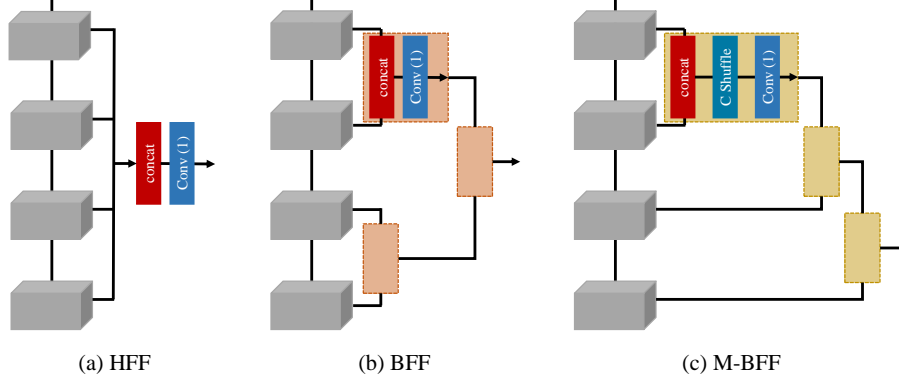


Fig. 4: Comparison of different feature fusion structures (1) HFF [28], (2) BFF [32], (3) M-BFF (Ours). In figure ‘concat’ refers to channel-wise concatenation, ‘Conv(1)’ refers to 1×1 convolution, and ‘C Shuffle’ shows channel shuffle

3.1 Feature Fusion Group (FFG)

Our proposed FFG has m multi-attention blocks (MAB). The details of MAB are discussed in the next section. The proposed MABs are combined through a modified form of binarized feature fusion (BFF) structure [32]. HFF [28] is another fusion structure that is commonly used though during experiments we found that BFF [32] performs better than HFF [28] (details are discussed in section 4.1). We refer to modified BFF as M-BFF. The comparisons of structures are shown in Figure 4. In BFF, all the adjacent blocks are separately concatenated like a binary tree structure. In contrast, our M-BFF concatenates the resultant feature block with the next MAB as shown on the left side of Figure 3. By taking the inspiration from ShuffleNet [49] that applies a channel shuffle method to mix the information among groups, we introduce the channel shuffle to mix the information between concatenated channels followed by a channel reduction layer that reduces the channels to make it equal to the number of input channels. In the end, we element-wise add the input features to the output features. Additionally, the residual connections may contain redundant information, thus to filter desired and useful information we multiply the results with trainable parameters λ_1^n and λ_2^n where n refers to n^{th} FFG.

3.2 Multi-attention Block (MAB)

In this section, we define the details of our proposed residual block, called MAB. [50] has emphasized the importance of channel attention (CA) mechanism. Consequently, many SR methods have focused on attention mechanisms, mainly CA and spatial attention (SA) [43,23,32]. Recently, [30] proposed a combined solution for CA and SA called enhanced spatial attention (ESA). The ESA block

reduces the number of channels with 1×1 convolutions and the number of spatial size with strided convolutions. Later, these spatial and channel sizes are increased to match the input size. Lastly, sigmoid operation is applied to get a similar effect as channel attention mechanism [17].

We modify the ESA block to make it more efficient by introducing dilated convolutions with different filter sizes. Further, we element-wise add all output features of dilated convolutions together to minimize the gridding effects [44]. The dilated convolutions not only reduce our memory computations but also increase spatial filter sizes, enabling us to improve the performance. Further, we introduce another cost-efficient attention mechanism (CEA) [4] to refine our input features. The CEA consists of point-wise and depth-wise convolutions. It is incorporated into the MAB block to improve the performance of our network with the negligible additional computational cost. The structure of MAB is presented on the right side of Figure 3.

4 Experimental Setup

Implementation Details

As we focus on developing a lightweight model, we aim to maximize the performance of existing networks as well as minimize their computational cost. We denote our original model as MAFFSRN. Further, we also introduce our larger model MAFFSRN-L to show that we can enhance the performance of our model depending on the available computing resources.

Our lightweight model MAFFSRN consists of 4 FFGs and 4 MABs whereas, for MAFFSRN-L model, we keep the same number of MABs and increase the FFGs to 8. We reduce the number of channels by a factor of 4 in MAB and set stride=3 to reduce the spatial size. The dilatation factors are set to $D = 1$ and $D = 2$. The values of scale λ are initialized with 0.5. We set the number of filters to 32 for every Conv layer except the last layer. For the last layer, we use 3 filters to reconstruct 3-color images. It can be modified to 1 filter for grayscale images.

Training Settings

We used AdamP optimizer [15] to train our models with initial learning rate 2×10^{-4} . For the data augmentations, we apply standard techniques i.e., images are flipped horizontally or vertically and randomly rotated by 90° , 180° and 270° . The models are trained for 1000 epochs and learning rate is decreased to half after every 200 epochs. We set batch-size to 16 and input patch size to 48×48 . We implement our network on PyTorch and train it on NVIDIA RX 2080TI GPU and select the best performance model.

Datasets

We use the high-quality DIV2K [1] dataset for training our models. It consists of LR and HR pairs of 800 training images. The LR images are obtained through

bicubic down-sampling. For the evaluation of our models, we use the standard and publicly available benchmark datasets, Set5 [3], Set14 [45], B100 [31], and Urban100 [19] datasets. Set5 [3], Set14 [45], B100 [31] contain animals, people, and natural scenes, while Urban100 [19] consists of urban scenes only.

Evaluation metrics

We measure the performance of reconstructed SR images with PSNR and SSIM [42] by following [21], using luminance or Y-channel of transformed YCbCr color space. We also calculate the number of parameters and multi-adds to compare the computational complexity of proposed models with existing methods.

Table 1: Effects of BFF, M-BFF, and CEA modules. Experiments are performed on Set5 (2×)

BFF	M-BFF	CEA	PSNR/SSIM	Parameters
X	X	X	37.87/0.9601	364K
✓	X	X	37.91/0.9602	372K
X	✓	X	37.94/0.9602	372K
X	X	✓	37.93/0.9603	394K
X	✓	✓	37.97/0.9603	402K

4.1 Ablation Studies

We conduct a series of ablation studies to demonstrate the importance of each proposed module used in our model. For all these experiments, we fully train our MAFFSRN model for 1000 epochs. In the first experiment, we train multiple models with similar settings to show the overall contribution of M-BFF and CEA. Each time we remove one component and test the network performance without that specific module. The results are shown in Table 1. It is noted that the model without M-BFF refers to model with HFF [27] structure that is a common choice for SR methods. Row 2 of Table 1 suggests that M-BFF improves 0.07 dB PSNR with only 8K additional parameters. Similarly, CEA adds 0.05 dB with 32K parameters. Lastly, when we combine CEA and M-BFF, our model obtains 0.1 dB PSNR with less than 40K additional parameters. Note, for the fair comparisons, we add channel shuffle in all three methods.

To demonstrate the importance of channel shuffle in our proposed MAFFSRN, we remove channel shuffle from MAFFSRN and report the results in Table 2. The results clearly indicate that with channel shuffle, we can increase the performance up to 0.04 PSNR.

For further evaluation, we experimented with a different type of Conv layers to show the efficacy of dilated convolutions in MAB. The experimental results in Table 3 suggest that our dilated convolutions perform better results than three

Table 2: Importance of channel shuffle in MAFFSRN. Experiments are performed on Set5 ($2\times$)

Method	PSNR/SSIM
Without Channel Shuffle	37.93/0.9603
With Channel Shuffle (Ours)	37.97/0.9603

Table 3: Evaluation of performance of different Conv layers in MAB. Here ‘d’ represents dilation factors. Experiments are performed on Set5 ($2\times$) with MAFFSRN

Number of Conv Layers	Details	PSNR/SSIM	Params
2 (ours)	3x3, 3x3 (d=2)	37.97 /0.9603	402394
2	3x3, 3x3	37.95/0.9603	402394
3	3x3, 3x3,3x3	37.96/ 0.9604	411738
2	3x3, 5x5	37.89/0.9602	418778
2	5x5, 3x3	37.92/0.9602	418778

convolutions and, surprisingly, methods having 5×5 convolutions are the worst performances. The reason could be the structure of the Conv layers as element-wise addition of 3×3 and 5×5 Conv layers has no significant benefits over dilated convolutions that utilize both layers more effectively.

We further experimented to compare the Adam [24] and AdamP [15] in Table 4 and found that AdamP [15] consistently outperforms the Adam[24] optimizer on all of the datasets with a large margin.

Table 4: Performance comparison between Adam [24] and AdamP[15]

Optimizer	Set5 [3]	Set14[45]	B100 [31]	Urban100 [19]
	PSNR/SSIM	PSNR/SSIM	PSNR/SSIM	PSNR/SSIM
Adam[24]	37.87/0.9601	33.42/0.9165	32.09/0.8987	31.75/0.9245
AdamP[15]	37.97/0.9603	33.49/0.9170	32.14/0.8994	31.96/0.9268

4.2 Comparison with Existing Methods

In this section, we present our quantitatively and qualitatively results and compare their performance with the state-of-the-art methods [8,10,21,22,33,25,35,11,5,7,48,2,52] on three up-scaling factors $2\times$, $3\times$ and $4\times$. The quantitative results are shown in Table 5. These also include the number of operations (Multi-Adds) and number of parameters to show the model complexity. Multi-Adds are estimated on 720p HR image. The results suggest that our lightweight MAFFSRN model achieves better performance than other methods on multiple datasets and scaling factors. Note that, our lightweight MAFFSRN model shows comparable performance to those models that consume $2\times$ to $3\times$ computing resources.

Table 5: Quantitative comparisons of existing methods on four datasets and three scales 2 \times , 3 \times , and 4 \times . Red/blue/green text: best/second-best/third-best

Scale	Model	Params	Multi-Adds	Set5	Set14	B100	Urban100
				PSNR/SSIM	PSNR/SSIM	PSNR/SSIM	PSNR/SSIM
2	SRCNN[8]	57K	52.7G	36.66/0.9542	32.42/0.9063	31.36/0.8879	29.50/0.8946
	FSRCNN[10]	12K	6.0G	37.00/0.9558	32.63/0.9088	31.53/0.8920	29.88/0.9020
	VDSR[21]	665K	612.6G	37.53/0.9587	33.03/0.9124	31.90/0.8960	30.76/0.9140
	DRCN[22]	1,774K	17,974.3G	37.63/0.9588	33.04/0.9118	31.85/0.8942	30.75/0.9133
	CNF[33]	337K	311.0G	37.66/0.9590	33.38/0.9136	31.91/0.8962	-
	LapSRN[25]	813K	29.9G	37.52/0.9590	33.08/0.9130	31.80/0.8950	30.41/0.9100
	DRRN[35]	297K	6,796.9G	37.74/0.9591	33.23/0.9136	32.05/0.8973	31.23/0.9188
	BTSRN[11]	410K	207.7G	37.75/-	33.20/-	32.05/-	31.63/-
	MemNet[35]	677K	2,662.4G	37.78/0.9597	33.28/0.9142	32.08/0.8978	31.31/0.9195
	SelNet [5]	974K	225.7G	37.89/0.9598	33.61/0.9160	32.08/0.8984	-
	FALSR-A[7]	1,021K	234.7G	37.82/0.9595	33.55/0.9168	32.12/0.8987	31.93/0.9256
	FALSR-B[7]	326K	74.7G	37.61/0.9585	33.29/0.9143	31.97/0.8967	31.28/0.9191
	FALSR-C[7]	408K	93.7G	37.66/0.9586	33.26/0.9140	31.96/0.8965	31.24/0.9187
	SRMDNF[48]	-	-	37.79/0.9601	33.32/0.9159	32.05/0.8985	31.33/0.9204
	CARN [2]	1,592K	222.8G	37.76/0.9590	33.52/0.9166	32.09/0.8978	31.92/0.9256
	CARN-M [2]	412K	91.2G	37.53/0.9583	33.26/0.9141	31.92/0.8960	31.23/0.9193
	CBPN-S[52]	430K	101.5G	37.69/0.9583	33.36/0.9147	32.02/0.8972	31.55/0.9217
	CBPN[52]	1,036K	240.7G	37.90/0.9590	33.60/0.9171	32.17/0.8989	32.14/0.9279
	MAFFSRN (ours)	402K	77.2G	37.97/0.9603	33.49/0.9170	32.14/0.8994	31.96/0.9268
	MAFFSRN-L (ours)	790K	154.4G	38.07/0.9607	33.59/0.9177	32.23/0.9005	32.38/0.9308
3	SRCNN[8]	57K	52.7G	32.75/0.9090	29.28/0.8209	28.41/0.7863	26.24/0.7989
	FSRCNN[10]	12K	5.0G	33.16/0.9140	29.43/0.8242	28.53/0.7910	26.43/0.8080
	VDSR[21]	665K	612.6G	33.66/0.9213	29.77/0.8314	28.82/0.7976	27.14/0.8279
	DRCN[22]	1,774K	17,974.3G	33.82/0.9226	29.76/0.8311	28.80/0.7963	27.15/0.8276
	CNF[33]	337K	311.0G	33.74/0.9226	29.90/0.8322	28.82/0.7980	-
	DRRN[35]	297K	6,796.9G	34.03/0.9244	29.96/0.8349	28.95/0.8004	27.53/0.8378
	BTSRN[11]	410K	176.2G	34.03/-	29.90/-	28.97/-	27.75/-
	MemNet[36]	677K	2,662.4G	34.09/0.9248	30.00/0.8350	28.96/0.8001	27.56/0.8376
	SelNet[5]	1,159K	120.0G	34.27/0.9257	30.30/0.8399	28.97/0.8025	-
	SRMDNF[48]	-	-	34.12/0.9254	30.04/0.8382	28.97/0.8025	27.57/0.8398
	CARN [2]	1,592K	118.8G	34.29/0.9255	30.29/0.8407	29.06/0.8034	28.06/0.8493
	CARN-M [2]	412K	46.1G	33.99/0.9236	30.08/0.8367	28.91/0.8000	27.55/0.8385
	MAFFSRN (ours)	418K	34.2G	34.32/0.9269	30.35/0.8429	29.09/0.8052	28.13/0.8521
	MAFFSRN-L (ours)	807K	68.5G	34.45/0.9277	30.40/0.8432	29.13/0.8061	28.26/0.8552
4	SRCNN[8]	57K	52.7G	30.48/0.8628	27.49/0.7503	26.90/0.7101	24.52/0.7221
	FSRCNN[10]	12K	4.6G	30.71/0.8657	27.59/0.7535	26.98/0.7150	24.62/0.7280
	VDSR[21]	665K	612.6G	31.35/0.8838	28.01/0.7674	27.29/0.7251	25.18/0.7524
	DRCN[22]	1,774K	17,974.3G	31.53/0.8854	28.02/0.7670	27.23/0.7233	25.14/0.7510
	CNF[33]	337K	311.0G	31.55/0.8856	28.15/0.7680	27.32/0.7253	-
	LapSRN[25]	813K	149.4G	31.54/0.8850	28.19/0.7720	27.32/0.7280	25.21/0.7560
	DRRN[35]	297K	6,796.9G	31.68/0.8888	28.21/0.7720	27.38/0.7284	25.44/0.7638
	BTSRN [11]	410K	165.2G	31.85/-	28.20/-	27.47/-	25.74/-
	MemNet[35]	677K	2,662.4G	31.74/0.8893	28.26/0.7723	27.40/0.7281	25.50/0.7630
	SelNet[5]	1,417K	83.1G	32.00/0.8931	28.49/0.7783	27.44/0.7325	-
	SRDenseNet [38]	2,015K	389.9G	32.02/0.8934	28.50/0.7782	27.53/0.7337	26.05/0.7819
	SRMDNF[48]	-	-	31.96/0.8925	28.35/0.7787	27.49/0.7337	25.68/0.7731
	CARN [2]	1,592K	90.9G	32.13/0.8937	28.60/0.7806	27.58/0.7349	26.07/0.7837
	CARN-M [2]	412K	32.5G	31.92/0.8903	28.42/0.7762	27.44/0.7304	25.62/0.7694
	CBPN-S[52]	592K	63.1G	31.93/0.8908	28.50/0.7785	27.50/0.7324	25.85/0.7772
	CBPN[52]	1,197K	97.9G	32.21/0.8944	28.63/0.7813	27.58/0.7356	26.14/0.7869
	MAFFSRN (ours)	441K	19.3G	32.18/0.8948	28.58/0.7812	27.57/0.7361	26.04/0.7848
	MAFFSRN-L (ours)	830K	38.6G	32.20/0.8953	28.62/0.7822	27.59/0.7370	26.16/0.7887

Furthermore, to demonstrate the superiority of our model, we compare the performance (PSNR) and computational cost (Multi-Adds) of our models with the existing models in Figure 1. It is evident from figure that our methods outperform the existing networks in both complexity and PSNR. It is worth to

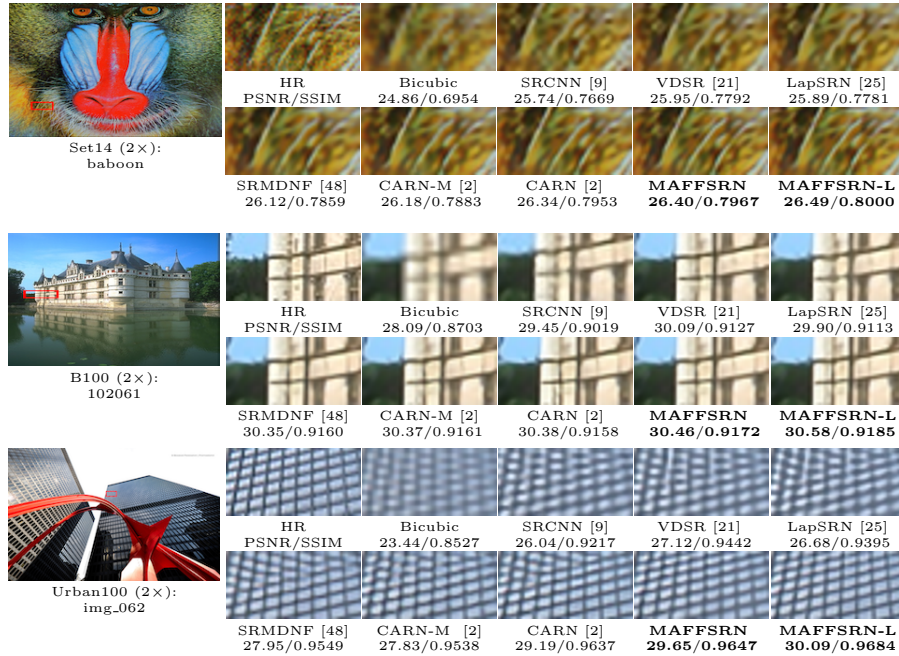


Fig. 5: Visual comparison for 2× SR with other models on Set14, B100, Urban10 dataset. The best results are **highlighted**

note that our MAFFSRN model even consists of fewer Multi-Adds than SRCNN [8] which is a shallow neural network with 3-layers.

We present our qualitative results in Figure 5 and Figure 6. In Figure 5, it can be seen from output results that the hairs of 'baboon' moustache are accurately reconstructed whereas other methods show blurry results. The similar effects can be seen in other images of Figure 5 where our methods demonstrate superior results. The results also include PSNR to show the qualitative results. Furthermore, our method continues to show improved results in even larger scale 4×. Overall, our methods have shown improved results as compared to existing methods.

5 AIM2020 Efficient SR Challenge

Our model is developed to participate in the AIM 2020 efficient SR challenge [46]. This competition targets to develop a practicable SR method that can be utilized in a constrained environment. The aim was to maintain the PSNR of MSResNet [41] on DIV2K [37] validation set while decreasing its computational cost. We submitted our MAFFSRN model to this challenge and won 1st in Memory computations, 3rd in FLOPs, 4th in number of parameters.

We present the results in Figure 7 and Table 6. Figure 7 shows the normalized scores on the y-axis and final participants on the x-axis. It also indicates

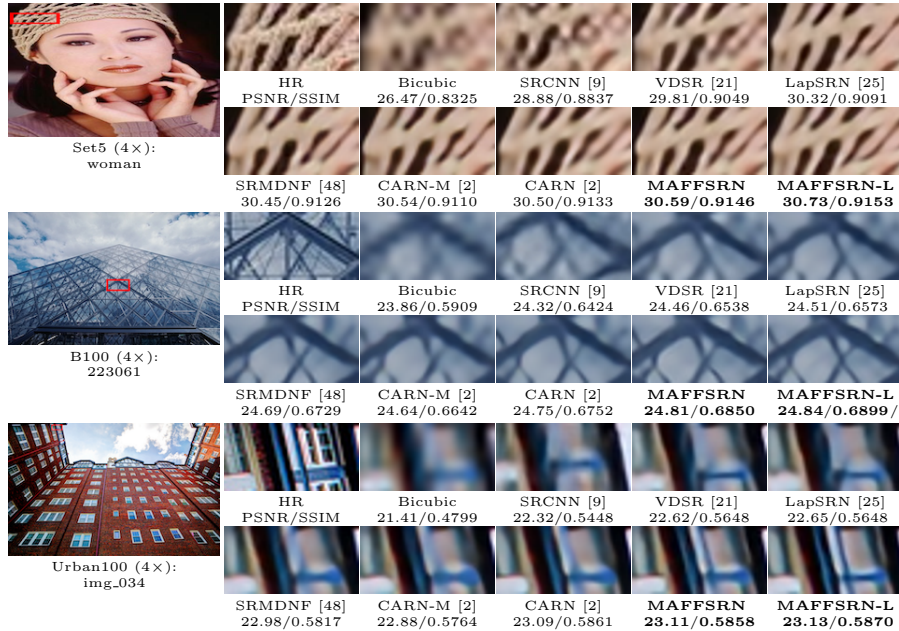


Fig. 6: Visual comparison for 4x SR with other models on Set5, B100, Urban100 dataset. The best results are **highlighted**

Table 6: Performance comparison of each entry in the AIM2020 efficient SR challenge. The number in the parenthesis denotes the rank

Method	Memory [MB]	FLOPs [G]	Parameters [M]
MAFFSRN	112(1)	27.11(3)	0.441(4)
Participant 1	146(2)	30.06(4)	0.461(5)
Participant 2	168(3)	44.98(9)	0.687(11)
Participant 3	200(4)	27.10(2)	0.433(3)
Participant 4	225(5)	49.67(10)	0.777(14)
Participant 5	229(6)	50.85(11)	0.761(13)
Baseline	610	166.36	1.517

that our proposed MAFFSRN model is a lightweight model among all participants. Similarly, we show the performance of top participants in Table 6 sorted by memory computations. Note that memory computations are tested with Pytorch code `torch.cuda.max_memory_allocated()` and FLOPs are calculated with an input image 256×256 .

6 Limitation and Future Work

In spite of having reduced computational cost (memory consumption, FLOPs, number of parameters), the runtime of the proposed method on the 100 val-

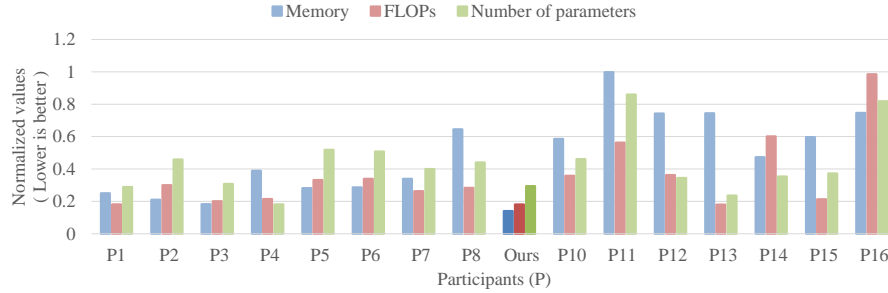


Fig. 7: Computational cost of all participants. Normalized values are shown on the x-axis whereas participants are shown on the y-axis. The results are shown in dark colors (ours) and light colors (other participants)

idation images of DIV2K dataset [37] is 0.104 sec per image³. The estimated runtime is averaged over 100 images. We assume it is a consequence of more layers in our networks than other efficient architectures. Nevertheless, the proposed method is ultra lightweight, and its memory-efficient modules can assist future researchers in the advancement of efficient SR architectures that have lower runtime and reduced memory consumption.

7 Conclusion

This work introduces a lightweight SR method for a constrained environment called MAFFSRN. We show with the several quantitative and qualitative experiments that MAFFSRN outperforms other existing lightweight models in terms of both performance and computational cost. Further, we present ablation studies to show the contributions of each proposed module.

Acknowledgement

This research was supported by Basic Science Research Program through the National Research Foundation of Korea (NRF) funded by the Ministry of Science, ICT & Future Planning (2018R1C1B3008159). Also, this research was a result of a study on the "HPC Support" Project, supported by the Ministry of Science and ICT and NIPA.

References

1. Agustsson, E., Timofte, R.: Ntire 2017 challenge on single image super-resolution: Dataset and study. In: Proc. Computer Vision and Pattern Recognition (CVPR) Workshops. pp. 126–135 (2017)

³ it is reported in [46]

2. Ahn, N., Kang, B., Sohn, K.A.: Fast, accurate, and lightweight super-resolution with cascading residual network. In: Proc. European Conference on Computer Vision (ECCV). pp. 252–268 (2018)
3. Bevilacqua, M., Roumy, A., Guillemot, C., Alberi-Morel, M.: Low-complexity single-image super-resolution based on nonnegative neighbor embedding. In: Proc. British Machine Vision Conference (BMVC). pp. 1–10 (2012)
4. Cai, Y., Wang, Z., Luo, Z., Yin, B., Du, A., Wang, H., Zhou, X., Zhou, E., Zhang, X., Sun, J.: Learning delicate local representations for multi-person pose estimation. arXiv preprint arXiv:2003.04030 (2020)
5. Choi, J.S., Kim, M.: A deep convolutional neural network with selection units for super-resolution. In: Proc. Computer Vision and Pattern Recognition (CVPR) Workshops. pp. 154–160 (2017)
6. Chollet, F.: Xception: Deep learning with depthwise separable convolutions. In: Proc. Computer Vision and Pattern Recognition (CVPR). pp. 1251–1258 (2017)
7. Chu, X., Zhang, B., Ma, H., Xu, R., Li, J., Li, Q.: Fast, accurate and lightweight super-resolution with neural architecture search. arXiv preprint arXiv:1901.07261 (2019)
8. Dong, C., Loy, C.C., He, K., Tang, X.: Image super-resolution using deep convolutional networks. Pattern Analysis and Machine Intelligence (PAMI) **38**(2), 295–307 (2015)
9. Dong, C., Loy, C.C., He, K., Tang, X.: Image super-resolution using deep convolutional networks. Pattern Analysis and Machine Intelligence (PAMI) **38**(2), 295–307 (2016)
10. Dong, C., Loy, C.C., Tang, X.: Accelerating the super-resolution convolutional neural network. In: Proc. European Conference on Computer Vision (ECCV). pp. 391–407. Springer (2016)
11. Fan, Y., Shi, H., Yu, J., Liu, D., Han, W., Yu, H., Wang, Z., Wang, X., Huang, T.S.: Balanced two-stage residual networks for image super-resolution. In: Proc. Computer Vision and Pattern Recognition (CVPR) Workshops. pp. 161–168 (2017)
12. Han, S., Mao, H., Dally, W.J.: Deep compression: Compressing deep neural networks with pruning, trained quantization and huffman coding. arXiv preprint arXiv:1510.00149 (2015)
13. Haris, M., Shakhnarovich, G., Ukita, N.: Deep back-projection networks for super-resolution. In: Proc. Computer Vision and Pattern Recognition (CVPR) (2018)
14. He, K., Zhang, X., Ren, S., Sun, J.: Deep residual learning for image recognition. In: Proc. Computer Vision and Pattern Recognition (CVPR). pp. 770–778 (2016)
15. Heo, B., Chun, S., Oh, S.J., Han, D., Yun, S., Uh, Y., Ha, J.W.: Slowing down the weight norm increase in momentum-based optimizers. arXiv preprint arXiv:2006.08217 (2020)
16. Hinton, G., Vinyals, O., Dean, J.: Distilling the knowledge in a neural network. arXiv preprint arXiv:1503.02531 (2015)
17. Hu, J., Shen, L., Sun, G.: Squeeze-and-excitation networks. In: Proc. Computer Vision and Pattern Recognition (CVPR). pp. 7132–7141 (2018)
18. Huang, G., Liu, Z., Van Der Maaten, L., Weinberger, K.Q.: Densely connected convolutional networks. In: Proc. Computer Vision and Pattern Recognition (CVPR). pp. 4700–4708 (2017)
19. Huang, J.B., Singh, A., Ahuja, N.: Single image super-resolution from transformed self-exemplars. In: Proc. Computer Vision and Pattern Recognition (CVPR). pp. 5197–5206 (2015)
20. Ioffe, S., Szegedy, C.: Batch normalization: Accelerating deep network training by reducing internal covariate shift. arXiv preprint arXiv:1502.03167 (2015)

21. Kim, J., Lee, J.K., Lee, K.M.: Accurate image super-resolution using very deep convolutional networks. In: *cvpr* (June 2016)
22. Kim, J., Lee, J.K., Lee, K.M.: Deeply-recursive convolutional network for image super-resolution. In: *cvpr* (June 2016)
23. Kim, J.H., Choi, J.H., Cheon, M., Lee, J.S.: Ram: Residual attention module for single image super-resolution. *arXiv preprint arXiv:1811.12043* (2018)
24. Kingma, D.P., Ba, J.: Adam: A method for stochastic optimization. *arXiv preprint arXiv:1412.6980* (2014)
25. Lai, W.S., Huang, J.B., Ahuja, N., Yang, M.H.: Deep laplacian pyramid networks for fast and accurate super-resolution. In: *cvpr* (2017)
26. Ledig, C., Theis, L., Huszár, F., Caballero, J., Cunningham, A., Acosta, A., Aitken, A., Tejani, A., Totz, J., Wang, Z., et al.: Photo-realistic single image super-resolution using a generative adversarial network. In: *Proc. Computer Vision and Pattern Recognition (CVPR)*. pp. 4681–4690 (2017)
27. Li, J., Fang, F., Mei, K., Zhang, G.: Multi-scale residual network for image super-resolution. In: *Proc. European Conference on Computer Vision (ECCV)*. pp. 517–532 (2018)
28. Li, J., Fang, F., Mei, K., Zhang, G.: Multi-scale residual network for image super-resolution. In: *Proc. European Conference on Computer Vision (ECCV)* (September 2018)
29. Lim, B., Son, S., Kim, H., Nah, S., Lee, K.M.: Enhanced deep residual networks for single image super-resolution. In: *Proc. Computer Vision and Pattern Recognition (CVPR) Workshops* (July 2017)
30. Liu, J., Zhang, W., Tang, Y., Tang, J., Wu, G.: Residual feature aggregation network for image super-resolution. In: *Proc. Computer Vision and Pattern Recognition (CVPR)*. pp. 2359–2368 (2020)
31. Martin, D., Fowlkes, C., Tal, D., Malik, J.: A database of human segmented natural images and its application to evaluating segmentation algorithms and measuring ecological statistics. In: *Proc. International Conference on Computer Vision (ICCV)*. vol. 2, pp. 416–423. IEEE (2001)
32. Muqeet, A., Iqbal, M.T.B., Bae, S.H.: Hybrid residual attention network for single image super resolution. *arXiv preprint arXiv:1907.05514* (2019)
33. Ren, H., El-Khamy, M., Lee, J.: Image super resolution based on fusing multiple convolution neural networks. In: *Proc. Computer Vision and Pattern Recognition (CVPR) Workshops*. pp. 54–61 (2017)
34. Shi, W., Caballero, J., Huszár, F., Totz, J., Aitken, A.P., Bishop, R., Rueckert, D., Wang, Z.: Real-time single image and video super-resolution using an efficient sub-pixel convolutional neural network. In: *Proc. Computer Vision and Pattern Recognition (CVPR)*. pp. 1874–1883 (2016)
35. Tai, Y., Yang, J., Liu, X.: Image super-resolution via deep recursive residual network. In: *Proc. Computer Vision and Pattern Recognition (CVPR)* (2017)
36. Tai, Y., Yang, J., Liu, X., Xu, C.: Memnet: A persistent memory network for image restoration. In: *Proc. International Conference on Computer Vision (ICCV)* (2017)
37. Timofte, R., Agustsson, E., Van Gool, L., Yang, M.H., Zhang, L.: Ntire 2017 challenge on single image super-resolution: Methods and results. In: *Proc. Computer Vision and Pattern Recognition (CVPR) Workshops*. pp. 114–125 (2017)
38. Tong, T., Li, G., Liu, X., Gao, Q.: Image super-resolution using dense skip connections. In: *Proc. International Conference on Computer Vision (ICCV)*. pp. 4799–4807 (2017)

39. Urban, G., Geras, K.J., Kahou, S.E., Aslan, O., Wang, S., Caruana, R., Mohamed, A., Philipose, M., Richardson, M.: Do deep convolutional nets really need to be deep and convolutional? arXiv preprint arXiv:1603.05691 (2016)
40. Wang, C., Li, Z., Shi, J.: Lightweight image super-resolution with adaptive weighted learning network. arXiv preprint arXiv:1904.02358 (2019)
41. Wang, X., Yu, K., Wu, S., Gu, J., Liu, Y., Dong, C., Qiao, Y., Change Loy, C.: Esrgan: Enhanced super-resolution generative adversarial networks. In: Proc. European Conference on Computer Vision (ECCV). pp. 0–0 (2018)
42. Wang, Z., Bovik, A.C., Sheikh, H.R., Simoncelli, E.P., et al.: Image quality assessment: from error visibility to structural similarity. *IEEE transactions on image processing* **13**(4), 600–612 (2004)
43. Woo, S., Park, J., Lee, J.Y., So Kweon, I.: Cbam: Convolutional block attention module. In: Proc. European Conference on Computer Vision (ECCV). pp. 3–19 (2018)
44. Yu, F., Koltun, V., Funkhouser, T.: Dilated residual networks. In: Proc. Computer Vision and Pattern Recognition (CVPR). pp. 472–480 (2017)
45. Zeyde, R., Elad, M., Protter, M.: On single image scale-up using sparse-representations. In: International conference on curves and surfaces. pp. 711–730. Springer (2010)
46. Zhang, K., Danelljan, M., Li, Y., Timofte, R., et al.: Aim 2020 challenge on efficient super-resolution: Methods and results. In: European Conference on Computer Vision Workshops (2020)
47. Zhang, K., Gool, L.V., Timofte, R.: Deep unfolding network for image super-resolution. In: Proc. Computer Vision and Pattern Recognition (CVPR). pp. 3217–3226 (2020)
48. Zhang, K., Zuo, W., Zhang, L.: Learning a single convolutional super-resolution network for multiple degradations. In: Proc. Computer Vision and Pattern Recognition (CVPR). pp. 3262–3271 (2018)
49. Zhang, X., Zhou, X., Lin, M., Sun, J.: Shufflenet: An extremely efficient convolutional neural network for mobile devices. In: Proc. Computer Vision and Pattern Recognition (CVPR). pp. 6848–6856 (2018)
50. Zhang, Y., Li, K., Li, K., Wang, L., Zhong, B., Fu, Y.: Image super-resolution using very deep residual channel attention networks. In: Proc. European Conference on Computer Vision (ECCV). pp. 286–301 (2018)
51. Zhang, Y., Tian, Y., Kong, Y., Zhong, B., Fu, Y.: Residual dense network for image super-resolution. In: Proc. Computer Vision and Pattern Recognition (CVPR) (2018)
52. Zhu, F., Zhao, Q.: Efficient single image super-resolution via hybrid residual feature learning with compact back-projection network. In: Proceedings of the IEEE International Conference on Computer Vision Workshops (2019)